PCCP

PAPER

Cite this: *Phys. Chem. Chem. Phys.*, 2015, **17**, 30177

Spontaneous electric fields in solid carbon monoxide

Jérôme Lasne,[ab] Alexander Rosu-Finsen,[a] Andrew Cassidy,[c] Martin R. S. McCoustra[a] and David Field*[c]

Received 31st July 2015,
Accepted 21st September 2015

DOI: 10.1039/c5cp04536c

www.rsc.org/pccp

Reflection–absorption infrared spectroscopy (RAIRS) is shown to provide a means of observing the spontelectric phase of matter, the defining characteristic of which is the occurrence of a spontaneous and powerful static electric field within a film of material. The presence of such a field is demonstrated here through the study of longitudinal–transverse optical splitting in RAIR spectra in films of carbon monoxide, based upon the deposition temperature dependence of this splitting. Analysis of spectral data, in terms of the vibrational Stark effect, allows the measurement of the polarization of spontelectric films, showing for example that solid carbon monoxide at 20 K may maintain a spontelectric field of 3.78×10^{7} V m^{-1}, representing a polarization of 3.34×10^{-4} cm^{-2}. We comment on the astrophysical implications of polarized carbon monoxide ices, on the surface of cosmic grains in star-forming regions.

1. Introduction

When a molecular gas is condensed onto a substrate, a solid film may be formed which spontaneously exhibits a static electric field,[1–8] the strength of which may exceed 10^{8} V m^{-1}. Such spontaneously electrical solid films, so-called 'spontelectrics', represent a new structural and electrical phase of the solid state. The present work is devoted to a demonstration that RAIRS may be used to establish new spontelectric materials. This is illustrated here for solid carbon monoxide between 20 and 26 K.

The proof of principle of this method was provided recently through a RAIRS study of N_2O films.[8] Such films are known to be spontelectric,[1] through direct measurement of surface potentials, using an electron beam technique. Results in ref. 8 show that the spontelectric field may be detected by observing the vibrational Stark effect in the material, using RAIRS. The known strength and temperature dependence of the field in N_2O were used to reproduce the corresponding temperature dependence of the longitudinal–transverse optical (LO–TO) splitting. Here we invert the argument and use temperature dependence of the LO–TO splitting to obtain the spontelectric field in CO. The crux of the technique is that a measureable temperature dependence of the LO–TO splitting is diagnostic of the spontelectric nature of the film of material concerned.

On this basis, we use RAIRS to estimate the spontelectric parameters of solid CO, for which, in contrast to N_2O, no direct measurements of surface potentials have been made. In this study, we accordingly find that the LO–TO splitting in RAIR spectra of CO depends on the temperature of deposition, to the tune of $\sim$0.045 cm^{-1} K^{-1}. Measurements of the LO–TO splitting then allow the determination of the values of the spontelectric field as a function of film deposition temperature.

The reasons for pursuing this work are: (i) RAIRS is a technique available to many laboratories and RAIRS could therefore be used to investigate the possible spontelectric nature of many materials. (ii) There are potentially important astrophysical implications if CO is spontelectric.

Spontelectric materials discovered to date all possess a permanent dipole moment and range over simple hydrocarbons, halocarbons, alcohols, organic formates, benzene derivatives and such simple inorganics as nitrous oxide. Numerous data, outlined in ref. 1 and 7, and corresponding analyses, point to dipole orientation as the origin of the spontaneous polarization. This in turn gives rise to the electric fields observed. The salient properties of spontelectrics[1,6,7] are that (i) the spontelectric field is lower for higher deposition temperatures (but see [5]), (ii) the nature of the substrate, on which materials are condensed, has no bearing on the strength of the bulk spontelectric field, (iii) the value of the spontelectric field depends on both the nature of the material which is deposited and on the temperature at which the film is deposited, (iv) there exists a critical annealing temperature, termed the Curie point, by analogy with ferromagnetism, at which films depolarize and the spontelectric field disappears.

The presence of the spontelectric field results in a vibrational Stark effect in the solid, causing a shift in characteristic

[a] *Institute of Chemical Sciences, Heriot-Watt University, Riccarton, EH14 4AS Edinburgh, UK*
[b] *Laboratoire Interuniversitaire des Systèmes Atmosphériques (LISA), CNRS UMR 7583, Université Paris-Est Créteil, Université Paris Diderot, Faculté des Sciences et Technologie, 61 avenue du Général de Gaulle, 94010 Créteil Cedex, France*
[c] *Department of Physics and Astronomy, Aarhus University, DK-8000 Aarhus C, Denmark. E-mail: dfield@phys.au.dk*

vibrational frequencies.[8–12] Since the strength of the spontelectric field depends strongly on the temperature of deposition of the film of material, there is a corresponding temperature dependence of the vibrational frequencies measured using RAIRS. Based upon a model for the spontelectric effect,[1] we show in Section 3 that the apparent LO–TO splitting in solid CO has a significant contribution from the Stark effect arising from the spontelectric field. We find, for example, that at a deposition temperature of 20 K, the Stark effect contributes ~36% of the total measured splitting of 4.03 cm^{-1}. The observed temperature dependence of LO–TO splitting may be attributed wholly to the dependence of the spontelectric field on the film deposition temperature.[8]

For simplicity, we refer throughout to the observed splitting in RAIR spectra of CO films as LO–TO splitting. At the same time, we recognize that the absolute value of the splitting arises through a combination of the intrinsically different vibrational frequencies associated with LO and TO modes and, at the level of approximation adopted here, an independent contribution due to the vibrational Stark effect.

In the current work, spontelectric films are interrogated using RAIRS with a grazing infrared beam, such that the incident electric field of the beam has components both parallel and perpendicular to the film normal. Relative to the incident beam wavelength, the film can be considered infinite in the plane of the film and only transverse optical (TO) phonons can be excited in this plane. If however the thickness of the film is comparable to the wavelength of the incident beam, the boundary conditions allow for the excitation of longitudinal optical (LO) phonons along the normal axis. This is known as the Berreman effect,[13] and has been studied extensively in non-ionic films.[14–16] Longitudinal phonons resonate at higher frequencies, because of the induced field associated with longitudinal waves passing through a medium composed of dipolar species. Thus, LO–TO splitting occurs for vibrational modes, when an incident beam interrogates a thin film at a suitably oblique angle.

Henceforth ν_L and ν_T represent the frequencies for LO and TO phonons respectively and $\Delta\nu = \nu_L - \nu_T$ represents the value of the splitting. The force fields giving rise to ν_L and ν_T are modified by the vibrational Stark effect, through the presence of the spontelectric field. We show in Section 3 how we may relate the resulting modification of LO–TO splitting, and its temperature dependence, to the presence of a static spontelectric field, oriented along the surface normal of the film. Our analysis demonstrates how measurements of ν_L and ν_T may then lead to a full characterization of the spontelectric field in CO.

2. Experimental method and results

2.1 The experimental method

RAIRS experiments were performed in an ultrahigh vacuum system, described in detail elsewhere.[17,18] The substrate, an oxygen-free high conductivity copper block coated with a 300 nm amorphous silica layer,[19] is mounted on the end of a closed-cycle helium cryostat, reaching a base temperature of 18 K, measured with a KP-type thermocouple connected to an IJ-6 temperature controller (IJ Instruments). The central chamber is equipped with a line-of-sight quadrupole mass spectrometer (QMS, Hiden Analytical) and a Fourier-transform infrared spectrometer (Varian 670-IR) used in reflection–absorption mode, at a grazing incidence of 75° with respect to the normal to the substrate. After reflection from the sample, the infrared beam is focused into a liquid nitrogen cooled HgCdTe detector. The RAIR spectra presented here result from the co-addition of 512 spectra recorded at 0.1 cm^{-1} resolution. This high resolution was necessary to measure the small frequency shifts observed in RAIR spectra of solid CO films, recorded at different deposition temperatures.

Films are deposited by background dosing of CO gas (BOC, purity 99.9%) onto the substrate at a rate of 0.05 ML s^{-1}. Thicknesses of CO films in monolayers (ML) were determined (±20%) through temperature-programmed desorption experiments, performed by applying a heating ramp of 0.3 K s^{-1} from the deposition temperature, with the desorbed species detected using the QMS.

The choice of the substrate was determined by the metal surface selection rule, which dictates that TO modes are silent on a metal surface. The presence of the silica layer coating, on the copper, relaxes this selection rule and allows the observation of both LO and TO modes in solid CO on silica, while retaining the enhanced sensitivity associated with RAIR spectroscopy. For a more detailed discussion in the case of N_2O films, see ref. 8.

2.2 Results

Fig. 1 presents the RAIR spectra of the νCO band of 5 ML CO films, deposited on 300 nm silica between 20 and 26 K. Increasing the deposition temperature red-shifts the LO mode, whilst the TO mode is blue-shifted. Annealing the films from 18 K to 26 K (not shown) does not produce any detectable shift of the bands. During the annealing experiments, desorption was

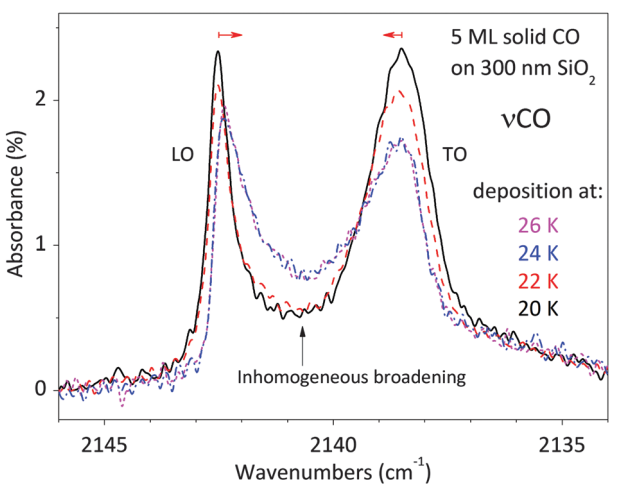

Fig. 1 RAIR spectra of 5 ML CO films deposited on 300 nm silica coated on a copper plate at 20 K (solid line), 22 K (dashed line), 24 K (dash-dotted line) and 26 K (short-dashed line).

negligible at and below 26 K, as confirmed by TPD and by the almost constant intensity of the RAIR signal of films annealed from 20 to 26 K.

LO–TO splitting can be observed at lower temperature than in the data shown here, that is, below 20 K. Evidence for volcano desorption from our substrate, during TPD of N_2O trapped in CO, is consistent with CO undergoing a phase change at around 20 K. Here RAIRS data are only presented for crystalline CO films, that is, for deposition temperatures $\geq$20 K, and the present study is therefore limited to a discussion of such crystalline films. The upper temperature boundary is set by the observation that films of CO form a steady state below 26 K, where the rate of desorption is low. Above 26 K the rate of desorption increases such that stable films cannot be grown.[20]

In the deposition experiments, the νCO LO and TO modes were fitted with Gaussian functions using the Igor Pro software. Fig. 2 presents the RAIR spectrum of a 5 ML CO film deposited at 20 K on 300 nm SiO_2 (open symbols), and the two Gaussian functions giving the best agreement with the experimental LO and TO modes (full lines). The inset of Fig. 2 shows the residuals, that is, the difference between the experimental spectrum and the fitting function, obtained in the LO mode region, with the best fit (full line) and after variation of the central position of the Gaussian by +0.01 (dotted line) and −0.01 cm^{-1} (dashed line). One can see that the residual is almost zero in the central region, and increases when going away from the maximum because of the inhomogeneous broadening of the bands. The flattest residual is obtained for a central position of 2142.52 cm^{-1}, that was hence considered the best fit for determination of the LO frequency at 20 K (see Table 2). A similar procedure was used for all determinations of LO and TO frequencies presented here. The uncertainties quoted above correspond to the maximum variation that can be applied to the central value of the fitted peak whilst maintaining the best match between the experimental spectrum and the fitted curve.

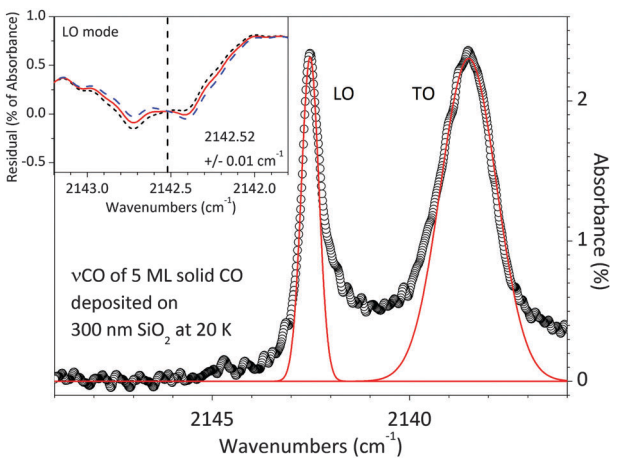

Fig. 2 RAIR spectrum of a 5 ML CO film deposited on 300 nm silica coated on a copper plate at 20 K (open symbols); Gaussian fits are shown with full lines. The inset shows the residuals of the fits of the LO mode: with a peak centred at 2142.52 (full line), 2142.53 (dotted line) or 2142.51 cm^{-1} (dashed line).

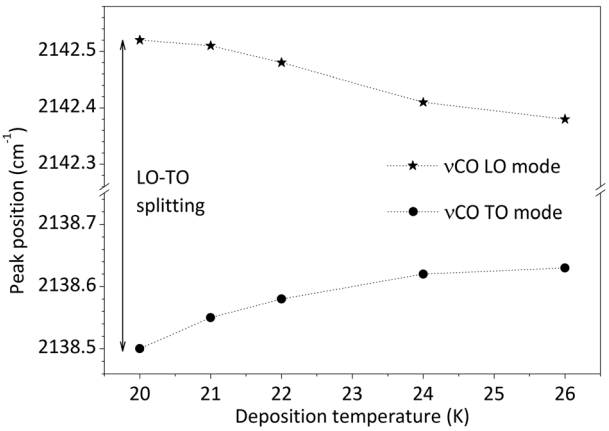

Fig. 3 Peak position of the νCO LO (stars) and TO (circles) modes of 5 ML CO films deposited on 300 nm silica, as a function of deposition temperature, deduced from fits to experimental data. The lines are a guide for the eye. Errors in frequencies are ±0.01 and ±0.02 cm^{-1} for LO and TO, respectively. Data are collated in Table 2, Section 3.1.

This method gives access to the uncertainty in the band position, yielding ±0.01 cm^{-1} for LO modes (see above and inset to Fig. 2) and ±0.02 cm^{-1} for the broader TO modes. The band positions resulting from the fits are displayed in Fig. 3 with stars and circles for the νCO LO and TO modes, respectively, for 5 ML CO films, deposited on 300 nm silica, as a function of deposition temperature.

We may also use the variation of the inhomogeneous broadening of LO and TO bands, with deposition temperature, as a qualitative indication of the degree of dipole orientation in the film. Fig. 4 shows a measurement of the inhomogeneous broadening of the νCO band for different deposition temperatures. The degree of broadening is estimated here by measuring the intensity of the RAIR spectrum at 2141 cm^{-1}, essentially the average frequency of the LO and TO modes, and normalizing by the integrated area of the band. This allows comparison

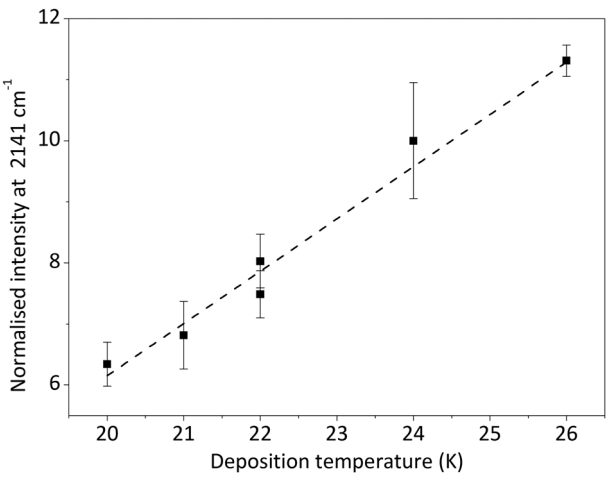

Fig. 4 Intensity measured at 2141 cm^{-1} in the RAIR spectra normalized by the total area of the νCO band for each spectrum, as a function of deposition temperature. The dotted line results from a linear fit of the data and is only presented here to guide the eye.

between different experiments and yields the ordinate in Fig. 4. Insofar as inhomogeneous broadening is a measure of the range of environments in which any component species finds itself, the greater the inhomogeneous broadening the less the dipole orientation. Results in Fig. 4 are therefore consistent with the expected behavior of a spontelectric material, and may be understood to show that the drop in dipole orientation increases with deposition temperature, as already observed in N_2O and numerous other films.[1,8]

3. A model for the spontelectric Stark effect

We first present qualitative evidence that CO films are indeed spontelectric. The LO–TO splitting changes from 4.02 cm^{-1} in 20 K films to 3.75 cm^{-1} at 26 K, noting that we have mentioned in the introduction that such variation is diagnostic of the presence of a temperature dependent spontelectric field in the film.

In ref. 8, we considered in detail for N_2O whether thermal expansion[14] could lead to the observed temperature variation of LO–TO splitting, $\Delta\nu$. Here, the measured average value of $d\Delta\nu/dT \sim -0.045$ cm^{-1} K^{-1} (see Table 2). Assuming that figures of density for solid CO are similar to those for N_2O, this would require a volume expansion coefficient for CO of between 0.002 and 0.003 K^{-1}, using the same analysis as that presented in Section 3.1.1 of ref. 8. However, low temperature volume expansion coefficients for such solid molecular materials typically lie between 10^{-5} and 10^{-6} K^{-1}. Therefore thermal expansion effects have a negligibly small influence on $\Delta\nu$. We conclude that the CO data presented here are *prima facie* evidence for the spontelectric nature of CO films.

We now seek to establish the spontelectric parameters of solid CO as a function of deposition temperature from the experimental data presented in Section 2. The most significant quantities, emerging from the subsequent analysis, are the values of the spontelectric field and the accompanying degrees of dipole orientation and of bulk polarization, as a function of the temperature of deposition.

In order to proceed, we first present our data in tabular form in Table 2 in Section 3.1. We use these data to evaluate the ratio of the Stark splitting contribution, $\Delta\nu_S$, to the full LO–TO splitting, $\Delta\nu$. In Section 3.2 we briefly review the necessary theoretical background for spontelectrics, identifying the symmetric field and asymmetric field parameters, $\langle E_{sym}\rangle$ and $\langle E_{asym}\rangle$ respectively, and defining the degree of dipole orientation. In Section 3.3, we develop explicit expressions relating $\Delta\nu_S$ to the spontelectric parameters and in Section 3.4 we extract values of the spontelectric field as a function of deposition temperature. For ease of reference, Table 1 shows the definition of the various symbols used here.

Table 1 Glossary of symbols used in Section 3

Symbol	Description
Terms obtained directly from experimental data	
ν_L	Longitudinal optical (LO) frequency
ν_T	Transverse optical (TO) frequency
$\Delta\nu$	Measured LO–TO splitting
$\Delta\nu_S$	Splitting due to the spontelectric Stark field
$\Delta\nu_B$	Intrinsic splitting
ξ	$\Delta\nu_S/\Delta\nu$
Terms involved in modelling	
μ	Dipole moment of CO in the solid state
$\langle\mu_z\rangle/\mu$	Degree of dipole orientation
Ω	Parameter related to the molecular volume of CO
T	Temperature of deposition
ζ	Locking term parameter in eqn (1)
E_S	Spontelectric field
$\langle E_{sym}\rangle$	Symmetric field parameter
$\langle E_{asym}\rangle$	Asymmetric field parameter = $(\langle\mu_z\rangle/\mu)/\varepsilon_0\Omega$

Table 2 Experimental data for solid CO: T: temperature of deposition, ν_T: transverse optical (TO) frequency, ν_L: longitudinal optical (LO) frequency, $\Delta\nu$ the LO–TO splitting, $\Delta\nu_S$: splitting due to the spontelectric Stark field and $\xi = \Delta\nu_S/\Delta\nu$

T/K	ν_T/cm^{-1} ±0.02	ν_L/cm^{-1} ±0.01	$\Delta\nu$/cm^{-1}	$\Delta\nu_S$/cm^{-1}	ξ
20	2138.50	2142.52	4.02	1.44	0.357
21	2138.55	2142.51	3.96	1.37	0.345
22	2138.58	2142.48	3.90	1.31	0.335
24	2138.62	2142.41	3.79	1.20	0.316
26	2138.63	2142.38	3.75	1.16	0.308

3.1 Contributions of the intrinsic effect and the Stark effect to the LO–TO splitting

The data shown in Fig. 3 are shown numerically in Table 2. The first three columns of Table 2 summarize RAIRS spectroscopic data, for LO–TO frequencies in solid CO, as a function of deposition temperature, T. These data are shown in Fig. 3. Column 4 of Table 1 shows the LO–TO splitting, $\Delta\nu$, that is, column 3–column 2.

$\Delta\nu$ may be represented by the sum of two terms, one of which, the intrinsic splitting, $\Delta\nu_B$, is independent of temperature of deposition, whereas the other, $\Delta\nu_S$, the spontelectric term, is a function of deposition temperature. Thus at any temperature $\Delta\nu = \Delta\nu_S + \Delta\nu_B$. We can use the data in Table 2 to determine an experimentally based value of $\Delta\nu_B$. This gives the desired values of $\Delta\nu_S$, as a function of temperature.

In order to estimate the relative contributions of $\Delta\nu_S$ and $\Delta\nu_B$ as a function of temperature, we invoke the concept that the spontelectric Stark field must tend to zero as the temperature is indefinitely raised, since at some temperature the system encounters the Curie point. In this connection we have found in earlier work on N_2O[1] that the mean field model, on which our current analysis is based, is inaccurate at the highest temperatures, close to sublimation. We note therefore at the outset that the data for CO at 26 K are somewhat anomalous. This is presumably because these data are taken very close to the limiting temperature at which CO can be condensed[20] and, by implication, in a regime in which fluctuations in the system begin to dominate and the mean field model becomes increasingly inapplicable.

$\Delta\nu_B$ is estimated by plotting $\Delta\nu$ *versus* $1/T$ and extrapolating to zero, that is, indefinitely high temperature. This is an *ad hoc* approach, based first on simplicity and second on the high

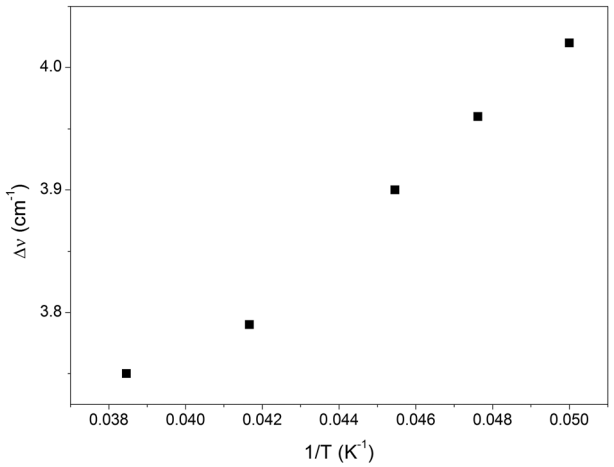

Fig. 5 $\Delta\nu$ *vs.* $1/T$, to obtain the value of $\Delta\nu_B$, using data at 20, 21, 22 and 24 K. Data at 26 K are shown for completeness. See Section 3.1 and Table 1.

accuracy with which data points, excluding data for 26 K, lie on a straight line, which may therefore be readily extrapolated. $\Delta\nu$ *versus* $1/T$ is shown in Fig. 5 in which the slope is linear to within 0.6% and the associated intercept to within 0.3%, ignoring the 26 K data. This yields an intercept at 2.59 ± 0.01 cm^{-1}, which is the value assigned throughout to $\Delta\nu_B$. The resulting values of $\Delta\nu_S$ and $\xi = \Delta\nu_S/\Delta\nu$ are shown in columns 5 and 6 of Table 2.

3.2 A brief resume of the model for the spontelectric effect

At this stage we need to introduce the theoretical model which governs spontelectrics. A detailed description may be found in ref. 1. This model successfully describes the variation with deposition temperature, of the observed spontelectric field, in films of N_2O, of N_2O diluted in xenon,[7] of methyl formate[5] and of CF_3Cl, CF_2Cl_2 and $CFCl_3$ films.[1] The model is based on the concept that the net z-component of the electric field within a spontelectric film and normal to the plane of the film, E_z, is composed of two parts. The first is a local symmetrical part, defining the interactions which both bind layers to one another and dictate the molecular force field and thus molecular vibrational frequencies. The second is an asymmetrical part, due to the long-range field which permeates the film. The symmetrical part is expressed as a constant term plus a dipole–dipole term, proportional to $(\langle\mu_z\rangle/\mu)^2$, representing average intermolecular dipole–dipole interactions. Here, $\langle\mu_z\rangle/\mu$, the degree of dipole orientation, is the ratio of the average z-component of the dipole moment and the total dipole moment of the molecular species in the solid state, where the *z*-axis is perpendicular to the plane of the film. The $(\langle\mu_z\rangle/\mu)^2$ form reflects the fact that all dipole interactions, involving dipole-image charge, extended dipoles and arrays of dipoles, follow this squared relation.[21–23] We note that the symmetrical part of the contribution to E_z is related to the 'local field' at any molecular site, as defined in standard texts.[24]

The asymmetrical part of E_z is described by $\langle E_{asym}\rangle\langle\mu_z\rangle/\mu$ and is equal to the observed spontelectric field. This term is found only in the description of spontelectrics, with no direct counterpart for any other form of material. This asymmetrical part resembles the Weiss field in ferromagnetism, which is assumed to be proportional to the magnetisation.[25] Here, read degree of dipole orientation for magnetisation and read polarisation field for the Weiss field. We emphasise that the polarisation field, that is, the spontelectric field, is self-generated within the spontelectric material. The polarization field acts in opposition to the symmetrical part and represents the long-range field created by the average dipoles and experienced by an average dipole. Note that this description highlights the non-linearity of the interactions involved.

The spontelectric field is a result of the macroscopic polarization, P, of the film of CO. In this connection, note the absence of any free charges in the film. If we write P_I as the polarization of a perfectly oriented system of dipoles, that is for $\langle\mu_z\rangle/\mu = 1$, then P_I is given in the limit of point dipoles by $P_I = \mu/\Omega$, where μ is the dipole moment of CO in the solid state, and Ω is a parameter related to the effective molecular volume of the CO molecule. So the true polarization is given by $(\langle\mu_z\rangle/\mu)\mu/\Omega$. Now $P = \varepsilon_0 E_S$, where E_S is the spontelectric field, noting that the use of ε_0 is appropriate since the dielectric effect of the medium has already been subsumed into the value of μ (see below). Thus $E_S = (\langle\mu_z\rangle/\mu)\mu/\varepsilon_0\Omega$ and $\langle E_{asym}\rangle = \mu/\varepsilon_0\Omega$ or $4\pi\mu/\Omega$ in atomic units. Ω is treated subsequently as a parameter to be obtained through analysis of the experimental data, effectively replacing the parameter $\langle E_{asym}\rangle$.

Hence, using atomic units throughout,

$$E_z = \langle E_{sym}\rangle\left[1 + \zeta\left(\frac{\langle\mu_z\rangle}{\mu}\right)^2\right] - E_S \qquad (1)$$

where $\langle E_{sym}\rangle$ and ζ are taken to be temperature independent parameters. The temperature dependence of the spontelectric field enters in general through the temperature dependence of both $\langle E_{asym}\rangle$ and $\langle\mu_z\rangle/\mu$. The $\zeta(\langle\mu_z\rangle/\mu)^2$ term in eqn (1) may be interpreted as a measure of the tendency of one dipolar species to restrict the angular motion of another, a 'locking' term or, as it is sometimes called, a 'frustration' term.

Mean field theory gives an implicit expression for $\langle\mu_z\rangle/\mu$, yielding the familiar Langevin function for orientational interactions[24]

$$\frac{\langle\mu_z\rangle}{\mu} = \coth\left(\frac{E_z\mu}{T}\right) - \left(\frac{E_z\mu}{T}\right)^{-1} \qquad (2)$$

where T is the deposition temperature of the layer of material and the Boltzmann constant is unity in atomic units. The dipole moment of CO in the solid state is reduced from that in the gas phase through depolarization in the environment of other CO species according to:

$$\mu = \frac{\mu_0}{1 + \alpha k/s^3} \qquad (3)$$

where s is the average spacing between successive layers, α is the molecular polarizability of CO (13.159 au), $k = 11.034$[26] and μ_0 is the gas phase dipole moment of CO (=0.122 D). s is estimated from the diameter of isoelectronic N_2 to be 0.339 nm or 6.406 au.

3.3 An explicit expression for $\Delta\nu_S$

The purpose here is to derive an expression for the contribution of $\Delta\nu_S$ to the LO–TO splitting, in terms of the spontelectric parameters introduced in Section 3.2. The first task is to combine eqn (1) and (2) to obtain an explicit expression for the degree of dipole orientation, $\langle\mu_z\rangle/\mu$.

We approximate the coth function in eqn (2) by expansion to first order, writing that $\coth(x) - 1/x = 1/3x$. Using values relevant to the present context, this approximation is accurate to better than one part in 10^5. We then obtain

$$\frac{\langle\mu_z\rangle}{\mu} = \frac{3T - 2\sqrt{\mu^2\zeta\langle E_{sym}\rangle(E_S - \langle E_{sym}\rangle) + 9T^2}}{2\mu\zeta\langle E_{sym}\rangle} \quad (4)$$

We now set out to express the LO–TO splitting in terms of spontelectric parameters. The internal electronic structure of the individual molecules, influenced by electrostatic effects from neighbouring molecules, is responsible for the force field associated with TO modes. Thus, $\langle E_{sym}\rangle[1 + \zeta(\langle\mu_z\rangle/\mu)^2]$, the first term of eqn (1), may be regarded as the average effective electric field at any molecule, giving rise to the force field which determines the value of νCO in the TO mode. However, the occurrence of a spontelectric field adds an additional potential in the direction normal to the plane of the film, shifting the LO vibrations to yet higher wavenumber than in intrinsic LO–TO splitting. Thus, the force field for LO includes an additional term involving the torque exerted on the molecular dipole in the spontelectric field. The field involved in this additional term has the form of the projection of the spontelectric field onto the direction in which the average dipole points, that is $E_S(\langle\mu_z\rangle/\mu)$. Dipole orientation also influences the force field dictating the TO mode, *via* the term $\langle E_{sym}\rangle\zeta(\langle\mu_z\rangle/\mu)^2$ in eqn (1) and the coupling of $\langle\mu_z\rangle/\mu$ to E_z in eqn (2).

Clearly the LO and TO modes possess two different effective force constants, reflecting the different force fields associated with LO and TO modes. Let k be the force constant associated with a fictitious solid, in the absence of either the spontelectric effect or effects leading to the intrinsic LO–TO splitting. Then in a real solid, two force constants may be encountered, $k - \delta_T$ and $k + \delta_L$ where, introducing the harmonic approximation, $\nu_L \propto (k + \delta_L)^{1/2}$ and $\nu_T \propto (k - \delta_T)^{1/2}$, recollecting that the LO frequency always lies higher than the TO frequency. We introduce the *ansatz* that $\delta_L = \delta_T = \delta$. This involves the assumption that the values of the parameters $\langle E_{sym}\rangle$, ζ and $\langle\mu_z\rangle/\mu$ are the same for both longitudinal and transverse modes. Given that $\delta \ll k$, we have shown in ref. 8 that

$$(U_L - U_T)/U_T \sim \Delta\nu/\nu_T \quad (5)$$

where U_T is the energy associated with the TO vibration and U_L with the LO vibration. In order to simplify the subsequent analysis, we have used $\Delta\nu/\nu_T \sim \Delta\nu/\nu_L$ in writing eqn (5). The overall accuracy of eqn (5) is better than 0.5%.

We now set out to relate the ratio of $U_L - U_T$ and U_T in eqn (5) to parameters governing the spontelectric effect. Consider first the total field at the molecule, corresponding to U_T, relevant to the TO mode. This total field includes that giving rise to both the local symmetric and spontelectric effects and may be represented by the term $\langle E_{sym}\rangle(1 + \zeta(\langle\mu_z\rangle/\mu)^2)$, in eqn (1). Since the ratio of the total field to the spontelectric part $\propto \xi^{-1}$, that is, $\Delta\nu/\Delta\nu_S$, the total splitting governing ν_T must itself be proportional to $\xi^{-1}\langle E_{sym}\rangle(1 + \zeta(\langle\mu_z\rangle/\mu)^2)$. Second, $U_L - U_T \propto$ the spontelectric field times the degree of dipole orientation, where this product gives the effective field. In each case there is an additional independent term describing the intrinsic LO–TO splitting, $\Delta\nu_B$. It then follows from eqn (5) that:

$$\frac{\Delta\nu}{\nu_T} \approx \frac{\xi^{-1}E_S(\langle\mu_z\rangle/\mu)}{\langle E_{sym}\rangle\left[\left(1 + \varsigma(\langle\mu_z\rangle/\mu)^2\right)\right]} + \frac{\Delta\nu_B}{\nu_T} \quad (6)$$

We now insert eqn (4) for $(\langle\mu_z\rangle/\mu)$ into eqn (6) giving, after some manipulation supplied by Mathematica,

$$\Delta\nu_S = \frac{\mu\xi\nu_T E_S T\left\{E_S\left[3T + \left(4\pi\mu^2\zeta\langle E_{sym}\rangle(E_S - \langle E_{sym}\rangle) + 9T^2\right)^{1/2}\right] - 6\langle E_{sym}\rangle T\right\}}{2\langle E_{sym}\rangle(E_S{}^2\mu^2\zeta + 9T^2)}\nu_T \quad (7)$$

where we have used $\Delta\nu_B = \Delta\nu - \Delta\nu_S$.

We now seek to solve eqn (7) for E_S, the spontelectric field. However the problem immediately arises that we have no value of the spontelectric parameters $\langle E_{sym}\rangle$ or ζ to use in eqn (7). To proceed we use

$$\Delta\nu_S = \frac{2\pi\mu\xi\left\{4\pi\mu^2 - \left[\left(9\Omega^2T^2 + 4\mu^2\left(4\pi^2\mu^2 - \Omega^2\zeta\langle E_{sym}\rangle^2 + 6\pi\Omega T\right)\right)^{1/2}\right] - 3\Omega T\right\}}{\Omega\zeta\langle E_{sym}\rangle(4\pi\mu^2 + 3\Omega T)}\nu_T \quad (8)$$

which is exactly equivalent to eqn (7) but in which we have used $E_S = (\langle\mu_z\rangle/\mu)\mu/\varepsilon_0\Omega$, inserting $\langle E_{asym}\rangle = 4\pi\mu/\Omega$ (Section 3.2) and we have employed

$$\frac{\langle\mu_z\rangle}{\mu} = \frac{\langle E_{asym}\rangle\mu + 3T\left[1 - \sqrt{\left(1 + \langle E_{asym}\rangle\mu/3T\right)^2 - 4\mu^2\zeta\langle E_{sym}\rangle^2/9T^2}\right]}{2\mu\zeta\langle E_{sym}\rangle} \quad (9)$$

which is equivalent to eqn (4). We note that since $E_S = (\langle\mu_z\rangle/\mu)\mu/\varepsilon_0\Omega$, we can write

$$\langle\mu_z\rangle/\mu = \Omega E_S/4\pi\mu \quad (10)$$

for ease of subsequent evaluation of the degree of dipole orientation, in place of eqn (4) or (9).

Our initial goal is therefore to find suitable values of the unknowns $\langle E_{sym}\rangle$, ζ and Ω, and hence $\langle \mu_z\rangle/\mu$, which satisfy our observations of $\Delta\nu_S$ as a function of deposition temperature. We make the assumption, based upon earlier work on modelling of spontelectric data,[1,7,8] that of the terms set out in Table 1, μ, ζ, $\langle E_{sym}\rangle$ are constant with temperature of deposition. In contrast to earlier work, we do not assume that $\langle E_{asym}\rangle$, or equally Ω, is constant with temperature of deposition. In Section 3.4.2, it is found that Ω may vary with temperature.

We proceed through four distinct steps.

(i) The first step is to make an estimate of $\langle E_{sym}\rangle$. We use eqn (8) to write down pairs of simultaneous equations, where each pair refers to a specific combination of two temperatures. These are then solved to yield six values of $\langle E_{sym}\rangle$ and Ω. The average value of $\langle E_{sym}\rangle$ is used in subsequent calculations.

(ii) In the second step, we use eqn (8) at all five different experimental temperatures and solve for Ω, using the average value of $\langle E_{sym}\rangle$ from step (i).

(iii) We solve eqn (7) to yield values of the spontelectric field, E_S.

(iv) We use eqn (10) to determine values of $\langle \mu_z\rangle/\mu$.

3.4 Extracting values of the spontelectric field as a function of deposition temperature

We now seek to use eqn (8) to obtain parameters of the spontelectric field. In order to simplify this procedure, we first take note that the value of $\Delta\nu_S$ in eqn (8) is insensitive to the value of ζ. We know from earlier work that ζ can assume a wide range of values,[1] from a few tens to $>10\,000$. However, numerical tests on eqn (8) show that variation of ζ over this range causes $\langle E_{sym}\rangle$ to vary by $<5\%$, given the values of the other parameters encountered here. This suggests the simplifying measure, which we adopt here, that ζ assumes some chosen value in the expected range and that the quantitative results of subsequent analysis are essentially independent of the value of this choice.

Physically, ζ determines the strength of the dipole locking term, as we have mentioned. Since the dipole moments in the solid state of CO and N_2O are essentially the same, respectively 0.0785 D and 0.0786 D, and the layer spacing is again similar, with $s_{N_2O} \sim 6.05$ au (0.32 nm) and $s_{CO} \sim 6.4$ au (0.34 nm), we have chosen to use the same value of ζ as derived from experimental data in ref. 1. Thus we adopt $\zeta = 43.8$, recognizing that the value could be reduced or increased by a factor of ten or more without making any significant difference to our conclusions.

3.4.1 Results of step (i): a solution for $\langle E_{sym}\rangle$. A typical example of a pair of simultaneous equations in $\langle E_{sym}\rangle$ and Ω, derived from eqn (8) for $T = 20$ and 24 K, are as follows:

$$1.44 = \frac{26.77 + \Omega\left[0.423 - 2228\sqrt{3.61\times10^{-8} + (1.44\times10^{-4} + 4.57\times10^{-6}\Omega)/\Omega^2 - 1.34\langle E_{sym}\rangle^2}\right]}{\Omega\langle E_{sym}\rangle(\Omega + 52.7)} \quad (11a)$$

and

$$1.20 = \frac{19.76 + \Omega\left[0.375 - 1644\sqrt{5.19\times10^{-8} + (1.44\times10^{-4} + 5.48\times10^{-6}\Omega)/\Omega^2 - 1.34\langle E_{sym}\rangle^2}\right]}{\Omega\langle E_{sym}\rangle(\Omega + 52.7)} \quad (11b)$$

which on solution gives $\langle E_{sym}\rangle = 8.79\times10^{-5}$ au or 4.52×10^{7} V m^{-1} and $\Omega = 11.8$ au. Note that we assume here that $\Omega_{20} = \Omega_{24}$, where the subscripts refer to temperature of deposition. This is discussed further in Section 3.4.2, but for the present we note that all pairs of equations give very similar values of $\Omega \sim 11.8$ au. It turns out in 3.4.2 below, that other values of Ω also satisfy the same values of $\langle E_{sym}\rangle$.

Taking values for all six combinations of data for $T = 20$, 21, 22 and 24 K, the average value of $\langle E_{sym}\rangle$ is found to be $4.48 \pm 0.21 \times 10^7$ V m^{-1}. The error quoted takes into account all experimental errors associated with ν_T and ν_L, $\pm$ 0.02 and 0.01 cm^{-1} respectively, coupled with an error in $\Delta\nu_B$ of 0.3% from data in Fig. 4 and an error of $\pm$0.25 K in the temperature of deposition. Note that in the above, we have excluded the data for 26 K in our analysis. As mentioned earlier, and as is plain in Fig. 5, data at 26 K appear somewhat anomalous and their inclusion in this step would add unnecessary additional numerical errors into our results.

3.4.2 Results of step (ii): solutions for Ω. We now use individual versions of eqn (8) at all six different experimental temperatures and solve for Ω, using the average value of $\langle E_{sym}\rangle = 4.48 \pm 0.21 \times 10^7$ V m^{-1} from step (i). The results of this procedure are shown in Table 4, illustrating that there are three values of Ω found for each temperature of deposition.

We see in Table 4 that Ω_1 and Ω_3 are approximately independent of temperature, ignoring the somewhat anomalous 26 K data. This is consistent with the assumption, used in evaluating $\langle E_{sym}\rangle$, that values of Ω at different temperatures can be equal. Analytically, it follows that values of Ω_2, whilst varying with temperature, are individually consistent with the constant value of $\langle E_{sym}\rangle$ used in the analysis. This has been checked numerically. One may note that the three different sets of values of Ω in Table 3 might be expected to emerge from step (i) above. This apparently does not materialise, for numerical reasons.

We now seek to choose between values of Ω_1, Ω_2 and Ω_3. Given that the polarization may be represented approximately by the dipole moment divided by the molecular volume (Section 3.2), then Ω should take on a value of the order of magnitude of the

Table 3 Values of the parameter Ω_1, Ω_2 and Ω_3 obtained from the solution of eqn (8), as function of the deposition temperature, T, where Ω_i are parameters related to the molecular volume of CO

T/K	Ω_1/au $\pm 0.16 \times 10^4$	Ω_2/au ± 7	Ω_3/au ± 0.3
20	5.34×10^4	341	11.8
21	5.45×10^4	310	11.8
22	5.52×10^4	282	11.8
24	5.69×10^4	236	11.8
26	5.77×10^4	194	12.2

molecular volume. A recent paper[27] reported the correlation between polarizability, α, and molecular volume and suggested the empirical relationship $\alpha = 0.0086161\ \Omega^{4/3}$. Using $\alpha = 13.159$ au, we find $\Omega = 244 \pm 30$ au. The average of Ω_2 in Table 3 is 273, favouring the choice of parameters associated with Ω_2. At the same time, one should beware of equating Ω_2 rigidly with the molecular volume, since results in Table 3 show that the value of this parameter changes rapidly with temperature, given the assumptions made in our analysis. We also note that $\Omega_1 \sim 5$ to 6×10^4 yields unphysical degrees of dipole orientation, greater than unity.

3.4.3 Results of step (iii): solutions for the spontelectric field. Solutions of eqn (7) for the spontelectric field are shown in Table 4, using data from Table 2 and again using the average value of $\langle E_{sym} \rangle = 4.48 \pm 0.21 \times 10^7$ V m^{-1} from step (i). Results in Table 4 show two values for the spontelectric field for each deposition temperature, the upper branch value E_{Su} and the lower, $E_{S\ell}$.

3.4.4 Results of step (iv): solutions for the degree of dipole orientation. Substituting values of E_{Su}, $E_{S\ell}$ and Ω_2 into eqn (10) yields values of $\langle \mu_z \rangle / \mu$ for each temperature. Results, subscripted u and ℓ are shown in Table 5, for the upper and lower spontelectric branches respectively.

In Table 5, consider first the upper branch, E_{Su}. This is well-behaved, in the sense that the spontelectric field declines as the temperature of deposition is raised and this is accompanied by a decline in dipole orientation. The lower branch, $E_{S\ell}$, by contrast shows the peculiar feature that the spontelectric field increases with temperature, accompanied however by the expected fall in dipole orientation. It may be possible to pursue the grounds for this behaviour through differentiation of eqn (7) with respect to T. This is not developed further here.

We now briefly compare our present results with data for the vibrational Stark shift of CO in the gas phase.[28] Following results reported in ref. 28, the fields presented in Table 5 would create a Stark shift of 0.93 ± 0.04 cm^{-1} and 0.19 ± 0.08 cm^{-1} for the upper and lower branch electric fields respectively, in the gas phase. We observe a shift of ~ 0.67 cm^{-1}, taking the average value of $\Delta\nu_S/2$. This serves to illustrate that our derived values of field are consistent with gas phase Stark data. However it leaves open the question of which of the two branches is relevant to the present experiment. On the basis that the Stark shift is likely to be lower in the solid state than in the gas phase due to depolarization, the above estimates would favour the higher value of spontelectric field, associated with the upper branch in Table 6. A comparison with data for N_2O, in Section 4 below, supports this suggestion.

We note that the double-valued, or multi-valued, behaviour, seen here in spontelectrics, is characteristic of non-linear, non-local systems, such as photonic crystals[29] where the bistability arises through non-linear Maxwell equations, to mention one of very many and varied examples. Moreover, this bimodal behaviour seen in spontelectrics – given that it is not some mathematical artefact – suggests new avenues of research. For example, the presence of two states represents a bi-metastable system, which may allow switching through an applied electric field. For the present, however, we do not explore this behaviour further, leaving it to future more detailed investigation. From hereon, we consider only the upper branch values of the spontelectric effect in Table 5.

Table 4 The upper, E_{Su}, and lower, $E_{S\ell}$, branch values of the spontelectric field in CO, obtained from eqn (7)

T	$E_{Su}/10^7$ V m^{-1} $\pm 0.15 \times 10^7$	$E_{S\ell}/10^6$ V m^{-1} $\pm 0.3 \times 10^6$
20	3.78	7.06
21	3.75	7.34
22	3.72	7.63
24	3.66	8.22
26	3.58	9.00

Table 5 The degree of dipole orientation, obtained from eqn (10), in the upper branch, $\langle \mu_z \rangle / \mu_u$, and in the lower branch, $\langle \mu_z \rangle / \mu_\ell$ of the spontelectric state of CO as a function of deposition temperature. Also shown are the upper, E_{Su}, and lower, $E_{S\ell}$, branch values for the spontelectric field (see Table 4)

T/K	$E_{Su}/10^7$ V m^{-1} $\pm 0.15 \times 10^7$	$\langle \mu_z \rangle / \mu_u$ ± 0.0024	$E_{S\ell}/10^6$ V m^{-1} $\pm 0.3 \times 10^6$	$\langle \mu_z \rangle / \mu_\ell$ ± 0.0001
20	3.78	0.0645	7.06	0.0121
21	3.75	0.0582	7.34	0.0114
22	3.72	0.0526	7.63	0.0108
24	3.66	0.0434	8.22	0.00971
26	3.58	0.0349	9.00	0.00876

4. Comparison with other spontelectric materials

The value of the spontelectric field in the upper branch of CO (Table 6) is comparable to that encountered in N_2O, the latter around a deposition temperature of ~ 60 K. The values of the

Table 6 Column 1: the material of which the spontelectric film is composed; column 2: deposition temperature of the material; column 3: number of mV added to the surface potential per ML of species deposited; column 4: corresponding degree of dipole orientation; column 5: gas phase dipole moment of species

Molecule	T/K	mV/ML	$\langle \mu_z \rangle / \mu$	μ_0/D	Ref.
CO	20	+12.8	0.0645	0.122	This work
Propane	40	−4.77	—	0.08	1 and 4
Propane	40	−0.72	—	0.08	1 and 4
Isopentane	40	−7.8	—	0.13	1 and 4
N_2O	40	+32	0.124	0.167	1 and 4
Isoprene	40	+35	—	0.25	1 and 4
Toluene	40	+6.5	—	0.385	1 and 4
CF_3Cl	40	−11.6	0.052	0.500	1, 4 and 6
CF_2Cl_2	45	−3.97	0.042	0.510	1 and 6
$CFCl_3$	43	−1.33	0.031	0.45	1 and 6
Methyl formate	40	5.78	0.0185	1.766	1 and 5

degree of dipole orientation in the upper branch are also similar to those encountered in N_2O in films, deposited between 52 and 65 K, which possess $\langle\mu_z\rangle/\mu$ = 0.0665 and 0.0204 respectively. The temperature of 65 K is close to the highest temperature at which deposition is possible for N_2O, much as is 26 K for CO. These remarks suggest some inherent similarity between the two species in their spontelectric properties. This may derive from their very similar values of dipole moment in the solid state, mentioned earlier.

The value of the spontelectric field for CO, expressed as mV of surface potential added per added monolayer, may be compared with values known for additional species, albeit typically at 40 K rather than 20 K. This comparison is illustrated in Table 6, where values for other species are taken from ref. 1. Values of the degree of dipole alignment are also shown in Table 6, where these are known. The significance of the data in Table 6 is to show that the characteristics, deduced for CO from RAIRS, fall into a bracket already encountered for spontelectrics. It is interesting to note that propane, in Table 6, explicitly shows a double valued nature,[1,4] switching from an upper branch to a lower branch at a film thickness of $\sim$2500 ML.

In addition, we can check our present method using data for N_2O. In ref. 8, as described in the introduction, we calculated the LO–TO splitting using spontelectric parameters for N_2O, known from earlier work based on direct measurement of the surface potential using the electron beam method. We then compared the measured LO–TO splitting at a variety of deposition temperatures, showing that the spontelectric Stark effect reproduces the LO–TO splitting data. We now test the use of the measured LO–TO splitting in N_2O, recorded in ref. 8, in reproducing the known degree of dipole orientation and the corresponding spontelectric field at temperatures between 48 and 60 K, using the analysis developed here.

We use the following parameters for N_2O: ζ = 75, Ω = 255 au, μ = 0.0785 D, the latter corresponding to a layer separation of 0.32 nm, taken from ref. 1. The value of Ω is that used in both ref. 1 and 8 and has been adopted here since we seek a comparison between different methods on the same footing. With data for ν_T, ξ and $\Delta\nu_S$ for N_2O taken from RAIRS data in ref. 8, we find, rearranging eqn (7), that the average value of $\langle E_{sym}\rangle$ is $4.69 \pm 0.19 \times 10^8$ V m^{-1}. This agrees within experimental error with the value of 4.57×10^8 V m^{-1}, reported in ref. 8. Note that the latter value was derived from fitting experimental data of surface potentials *vs.* temperature of deposition between 48 and 60 K for N_2O, reported in ref. 1, using the model outlined in Section 3.2.

We now use eqn (9) to calculate $\langle\mu_z\rangle/\mu$ as a function of temperature. Here $E_S = \langle E_{asym}\rangle\langle\mu_z\rangle/\mu = (\langle\mu_z\rangle/\mu)\mu/\varepsilon_0\Omega$, from eqn (10), yields the spontelectric field. Values are shown in column 5 of Table 7. The temperatures of deposition in Table 7 are selected to cover the range of values of experimental data available, using both the electron beam method and RAIRS. The second column of Table 7 shows values of $\langle\mu_z\rangle/\mu$ estimated from the present model, based, that is, upon RAIRS measurements. The third column shows results obtained using spontelectric parameters obtained by fitting to surface potential data,[1,8] using the theory outlined in Section 3.2. The fourth column presents values of dipole orientation derived from observational data in ref. 4. The three succeeding columns give corresponding values of the spontelectric field. The most telling comparison, for validation of the present model, is of values in columns two with those in three and those in five with those in six. Agreement with observational data, in columns 3 and 7, deteriorates at higher deposition temperature, reflecting the less accurate fitting for $\langle\mu_z\rangle/\mu_{calc}$ in this regime.

Table 7 Column 1: the film deposition temperature; column 2: the degree of dipole orientation calculated from RAIRS data; column 3: ditto estimated using the theory outlined in Section 3.2; column 4: ditto estimated from measured surface potentials. Columns 5–7: corresponding spontelectric fields

T/K	$\langle\mu_z\rangle/\mu$	$\langle\mu_z\rangle/\mu_{calc}$	$\langle\mu_z\rangle/\mu_{obs}$	$E_S/10^7$ V m^{-1}	E_S calc/10^7 V m^{-1}	E_S obs/10^7 V m^{-1}
48	0.0843	0.0826	0.0846	6.86	6.53	6.62
52	0.0732	0.0704	0.0665	5.96	5.57	5.21
57	0.0637	0.0615	0.0536	5.19	4.86	4.19
60	0.0594	0.0573	0.0467	4.84	4.53	3.66

Results in Table 7 validate the present method as it is applied here to CO. We note that values of the spontelectric field for N_2O in Table 7 appear consistently 5 to 7% higher, using the RAIRS data, than through numerical fitting to surface potential data.

5. A meeting point for condensed matter science and astrophysics

One may ask whether the existence of spontelectric CO has any consequence in the natural Universe. The reply is that this may well be the case, since interstellar dust grains could acquire a substantial polarization charge on the grain surface. This possibility is briefly explored below, for the most part qualitatively.

Without elaborating at length, it is well-established that interstellar grains in cold pre-stellar cloud cores are coated with an outer layer of quite pure solid CO (*e.g.* in Taurus[30]). The extent of this layer may be 50 to 60 ML, for example in the molecular core in L1544 in Taurus. We suppose below that the low rate of accumulation of CO in space has no influence on the spontelectric nature of the film formed.

Using figures from the present work, the spontelectric effect in CO at 20 K would generate a polarization potential of 0.7 V on such a grain, given a thickness of 50 to 60 ML. This potential is equivalent to a polarization charge of 50 electronic charges, noting that a grain is generally regarded as possessing typically one negative charge on its surface. Following ref. 31, which suggests that the positive O-end of CO would protrude from the surface, the polarization charge would be 50 positive.

It is evident that such a polarization charge would tend to attract electrons to the surface, altering the gas phase abundance of electrons. Using a density of grain material of 2 g cm^{-3} and a grain abundance by mass of 1.3%,[32] the proportion of electrons removed to the surface of the grains may be shown to be given by 1.06×10^{-25} $n_{ML}/(\alpha a^2)$, where n_{ML} is the number of

monolayers of CO, α is the degree of ionization and a is the grain radius. Values of α range[32] over a few 10^{-9} to $>10^{-8}$. Thus, say, if a = 0.025 μm and $\alpha = 10^{-8}$, then the degree of depletion of gas phase electrons would be >80%. This, in turn, would influence the abundance of chemical species in the interstellar medium. Molecular species, in particular water, are important for their cooling effect in a cloud under gravitational collapse and thus in maintaining such collapse approximately isothermal. There is an additional link to the chemistry through the nature of magnetic shocks, whose characteristics are strongly dependent on the gas phase abundance of electrons: see ref. 33 and 34 and references therein. Such shocks form both in star forming regions and close to the surface of nascent protostars.

Whilst the above suggests that the inclusion of spontelectric grains may have an influence on the chemistry and physics of the gravitational collapse of protostellar cores, a proper analysis requires a more complex – and interesting – kinetic approach than that suggested above. As CO is adsorbed, so the rate of electron adsorption will increase as the surface becomes more polarised.[35] At the same time, electro-neutrality of the plasma must be preserved, requiring an equal flux of positive ions and electrons to the grain surface. In connection with this, electron drag will pull positive ions towards the grains, leading to ambipolar diffusion. Coupled further with this, are the effects of a magnetic field, ~0.5 mG in L1544, which influences the motion of electrons. Future work in astrophysical modelling of star-forming clouds should therefore involve a time-dependent coupled magnetohydrodynamic and kinetic model in order to predict the time dependent effects of the presence of polarized grains in astrophysical plasma.

6. Concluding remarks

Our conclusions may be summarised as follows:

(i) As a standalone technique, RAIRS can be used to establish the spontelectric character of films. All that is required is the observation that the LO–TO splitting shows a measureable dependence on the film deposition temperature, and possibly also upon annealing when the effect is large enough. Data at a variety of deposition temperatures should then yield the strength of the spontelectric field and the degree of dipole orientation, as a function of film temperature. This would allow an exploration of the range of species which are spontelectric. RAIRS does not however inform us in which direction the field is oriented.

(ii) Our results call for new developments in modelling the chemistry and physics of pre- and protostellar cores, as part of the current extensive research into the nature of low-mass star formation and of planet-forming disks around young stars.[36]

Acknowledgements

We gratefully acknowledge support of the staff of the Aarhus 80 Synchrotron Radiation Laboratory (ISA), the Danish Research Council, European Community FP7-ITN Marie-Curie Programme (LASSIE project, grant agreement #238258; AC, JL), Heriot-Watt University for a James Watt scholarship (ARF) and the experimental assistance of Ms Holly Glenister.

References

1 D. Field, O. Plekan, A. Cassidy, R. Balog, N. C. Jones and J. Dunger, *Int. Rev. Phys. Chem.*, 2013, **32**, 345.
2 R. Balog, P. Cicman, N. Jones and D. Field, *Phys. Rev. Lett.*, 2009, **102**, 2.
3 D. Field, O. Plekan, A. Cassidy, R. Balog and N. Jones, *Europhys. News*, 2011, **42**, 32.
4 O. Plekan, A. Cassidy, R. Balog, N. C. Jones and D. Field, *Phys. Chem. Chem. Phys.*, 2011, **13**, 21035.
5 O. Plekan, A. Cassidy, R. Balog, N. C. Jones and D. Field, *Phys. Chem. Chem. Phys.*, 2012, **14**, 9972.
6 A. Cassidy, O. Plekan, R. Balog, N. C. Jones and D. Field, *Phys. Chem. Chem. Phys.*, 2012, **15**, 108.
7 A. Cassidy, O. Plekan, J. Dunger, R. Balog, N. C. Jones, J. Lasne, A. Rosu-Finsen, M. R. S. McCoustra and D. Field, *Phys. Chem. Chem. Phys.*, 2014, **16**, 23843.
8 J. Lasne, A. Rosu-Finsen, A. Cassidy, M. R. S. McCoustra and D. Field, *Phys. Chem. Chem. Phys.*, 2015, **17**, 20971.
9 S. A. Andrews and S. G. Boxer, *J. Phys. Chem. A*, 2002, **106**, 469.
10 E. S. Park and S. G. Boxer, *J. Phys. Chem. B*, 2002, **106**, 5800.
11 I. T. Suydam and S. G. Boxer, *Biochemistry*, 2003, **42**, 12050.
12 G. Schkolnik, J. Salewski, D. Millo, I. Zebger, S. Franzen and P. Hildebrandt, *Int. J. Mol. Sci.*, 2012, **13**, 7466.
13 D. Berreman, *Phys. Rev.*, 1963, **130**, 2193.
14 L. H. Jones and B. I. Swanson, *J. Phys. Chem.*, 1991, **95**, 2701.
15 M. A. Ovchinnikov and C. A. Wight, *J. Chem. Phys.*, 1993, **99**, 3374.
16 M. A. Ovchinnikov and C. A. Wight, *J. Chem. Phys.*, 1994, **100**, 972.
17 H. J. Fraser, M. P. Collings and M. R. S. McCoustra, *Rev. Sci. Instrum.*, 2002, **73**, 2161.
18 V. L. Frankland, A. Rosu-Finsen, J. Lasne, M. P. Collings and M. R. S. McCoustra, *Rev. Sci. Instrum.*, 2015, **86**, 055103.
19 J. D. Thrower, M. P. Collings, F. J. M. Rutten and M. R. S. McCoustra, *Mon. Not. R. Astron. Soc.*, 2009, **394**, 1510.
20 M. P. Collings, V. L. Frankland, J. Lasne, D. Marchione, A. Rosu-Finsen and M. R. S. McCoustra, *Mon. Not. R. Astron. Soc.*, 2015, **449**, 1826.
21 E. Cohen de Lara and J. Vincent-Geisse, *J. Phys. Chem.*, 1976, **80**, 1922.
22 B. L. Maschhoff and J. P. Cowin, *J. Chem. Phys.*, 1994, **101**, 8138.
23 D. Fernández-Torre, O. Kupiainen, P. Pyykkö and L. Halonen, *Chem. Phys. Lett.*, 2009, **471**, 239.
24 C. Kittel, *Introduction to Solid State Physics*, Wiley, 3rd edn, 2005.
25 H. Kliem, M. Kuehn and B. Martin, *Ferroelectrics*, 2010, **400**, 41.
26 J. Topping, *Proc. R. Soc. London, Ser. A*, 1927, **114**, 67.

27 S. A. Blair and A. J. Thakkar, *J. Chem. Phys.*, 2014, **141**, 074306.
28 S. S. Hashjin and C. F. Matta, *J. Chem. Phys.*, 2013, **139**, 144101.
29 J. D. Joannopoulos, S. G. Johnson, J. N. Winn and R. D. Meade, *Photonic Crystals; Molding the Flow of Light*, Princeton University Press, Princeton and Oxford, 2nd edn, 2008.
30 A. Brady Ford and Y. L. Shirley, *Astrophys. J.*, 2011, **728**, 144.
31 M. P. Collings, J. W. Dever and M. R. S. McCoustra, *Phys. Chem. Chem. Phys.*, 2014, **16**, 3479.
32 C. M. Walmsley, D. R. Flower and G. Pineau des Forêts, *Astron. Astrophys.*, 2004, 4181035.
33 H. D. Nissen, N. J. Cunningham, M. Gustafsson, J. Bally, J.-L. Lemaire, C. Favre and D. Field, *Astron. Astrophys.*, 2012, **540**, A119.
34 L. E. Kristensen, T. L. Ravkilde, G. Pineau des Forêts, S. Cabrit, M. Gustafsspn, S. Diana, J. L. Lemaire and D. Field, *Astron. Astrophys.*, 2008, **477**, 203.
35 B. T. Draine and B. Sutin, *Astrophys. J.*, 1987, **320**, 803.
36 N. Sakai, T. Sakai, T. Hirota, Y. Watanabe, C. Ceccarelli and C. Kahane, *et al.*, *Nature*, 2014, **507**, 78.